Proceedings of the ASME 2021 40th International
Conference on Ocean, Offshore and Arctic Engineering
OMAE2021
June 21-30, 2021, Virtual, Online

OMAE2021-62780

FOCUSED PLUNGING BREAKING WAVES IMPACT ON CYLINDER GROUP IN DEEP WATER

Ting Cui[1,2] **Arun Kamath**[2] **Weizhi Wang**[2] **Lihao Yuan**[1*] **Duanfeng Han**[1] **Hans Bihs**[2]

[1] College of Shipbuilding Engineering
Harbin Engineering University
Harbin 150001, China
Email: yuanlihao@hrbeu.edu.cn
[2] Marine Civil Engineering
Department of Civil and Environmental Engineering
Norwegian University of Science and Technology (NTNU)
Trondheim, Norway

ABSTRACT

The correct estimation of wave loading on a cylinder in a cylinder group under different impact scenarios is essential to determine the structural safety of coastal and offshore structures. This scenario differs from the interaction of waves with a single cylinder but not a lot of studies focus on cylinder groups under different arrangements. In this study, the interaction between plunging breaking waves and cylinder groups in deep water is investigated using the two-phase flow model in REEF3D, an open-source computational fluid dynamics program. The Reynolds-averaged Navier-Stokes equation with the two equation $k-\omega$ turbulence model is adopted to resolve the numerical wave tank, with free surface calculated using the level set method. In this study, focused waves in deep water were modeled with a fixed wave steepness method. Wave breaking occurs when the steepness of the wave crest front satisfies the breaking criteria. The model is validated by comparing the numerical wave forces and free surface elevation with measurements from experiments. The computational results show fairly good agreement with experimental data for both free surface elevation and wave forces. Four cases are simulated to investigate the interaction of breaking waves with a cylinder group with different relative distance, number of cylinders and arrangement. Results show that breaking wave forces on the upstream cylinder are smaller than on a single cylinder with a relative distance of one cylinder diameter. The wave forces on cylinders in the pile group are effected by the relative distance between cylinders. The staggered arrangement has a significant influence on the wave forces on the first and second cylinder. The interaction inside a cylinder group mostly happens between the neighbouring cylinders. These interactions are also effected by the relative distance and the numbers of the neighbouring cylinders.

INTRODUCTION

The focused breaking waves undergo steepness induced breaking, unlike the depth-induced breaking waves. This is a phenomenon occurring in the deeper waters in the offshore regions. The focused breaking waves occur generally as a result of non-linear irregular wave states where waves of different periods and heights can coincide at a certain location and time. The focused breaking waves usually carry large amount of energy and can cause several damages to offshore structures. With the development of deep ocean engineering, pile groups are the most utilised

support structures for fixed offshore marine structures e.g. offshore oil platforms, wind turbines and sea bridges, and play a significant role in the safe and cost-effective design of offshore structures. The interaction between a vertical cylinder and breaking waves alters the flow field, the kinematics and hydrostatics around a cylinder. To better understand the interaction between the focused breaking waves and pile groups in deep water, it is essential to study the extreme wave forces, kinematics transformation, flow field characteristics, the interaction scenario and arrangement of cylinders in a group.

The accurate prediction of the hydrodynamic loads on cylinders in a pile group is the most important part of offshore structural design. The Morison equation [1] and potential flow theory can provide an estimate of wave loads. However, in the situation of breaking waves, it is still a complex and challenging task especially with impact, splash-up and air entrainment. Goda [2] employed an additional wave force term to calculate wave forces under the wave breaking situation and obtained some good results. This theoretical method [3] relies on the incident wave characteristics, i.e. shape profile and velocity at the incipient point. A method proposed by [4] takes the effect of the beach slope into consideration when predicting the breaking wave forces on the vertical cylinder and has reasonable results for the depth induced breaking waves. For the case that the breaking waves induced by the steepness, this method loses its advantages.

The experiments provide a direct understanding of the interaction of breaking waves with the structures, especially for complex breaking scenarios. Watanabe et al. [5] investigated breaking wave forces on a cylinder and pointed out that the theoretical coefficients method used to calculate the wave forces are not correct under breaking wave conditions. A series of large-scale experiments were carried out using the Gaussian wave packet by [6] to examine the wave loading due to breaking wave impact on the single vertical cylinder. They found that the impact force on the cylinder is negligibly damped by entrapped air. Experiments to study the interaction between the focused breaking waves and a fixed vertical cylinder were performed by Zang [7] using the localized wave group method. The harmonic structures of the horizontal loading on the cylinder are still apparent even for the breaking waves and consistent with that measured for smaller non-breaking waves. Bing et al. [8] studied the focused plunging breaker impact on a single cylinder using the dispersive focusing method [9, 10] with a constant steepness spectrum. The experiment investigated the breaking wave forces on a single cylinder under different wave breaking stages and the experimental data was analysed with the FFT-EMD method. The maximum breaking wave forces were seen to be quite different under different scenarios in their results. However, measurements of the quantities such as velocity and acceleration related to the wave breaking and the interaction with the structures in the experiments is still demanding. A small-scale experiment was carried out by Bonakdar et al. [11] to investigate the pile group effect on the wave loading of a slender pile due to the nonbreaking and focused breaking waves. Different arrangements and distance between the members of the pile group were studied to investigate the influence of the group on the cylinders. They point out that the arrangements of pile groups with different angles with respect to the center line of the cylinder relative to the wave direction needs further investigation.

Some of meaningful numerical studies based on the CFD model have been performed to simulate the interaction of the breaking waves with a single vertical cylinder [12, 13, 14, 15, 16]. However, little attention has been paid to the pile group arrangement and the kinematic transformation around the interaction zone in deep water. Kamath et al. [17, 18] use the numerical model in REEF3D [19] to study the wave forces and flow profile around a group of the tandem vertical cylinders. The influence of the tandem arrangement on different scenarios on breaking wave forces of a pair of cylinders was investigated by Bihs et al. [20]. The numerical simulations carried out by Alagan Chella et al. [21] calculated the breaking wave forces on each of cylinders in a four-cylinder group. These studies also analysed the wave elevation and flow features around cylinders. These numerical simulations paid more attention to the interaction of the breaking waves with tandem cylinders and square arrangement pile group. The research on a staggered pile group and the spatial distance under the plunging breakers in deep water are not yet studied in detail.

The main purpose of this paper is to investigate interaction between the breaking waves and pile groups with different spatial distance and arrangements using the open source three-dimensional CFD model REEF3D. The free surface elevation and kinematic variation are studied. The two-equation $k-\omega$ model is adopted to model the turbulence. The numerical results are compared with the experimental data of the interaction between breaking wave and a vertical cylinder to validate the accuracy of the present model. The stretching refined grid reproduces reasonable results and reduces the computational cost. Four cases are performed to find out the influence of the pile group on the upstream and downstream cylinders on the focused plunging breakers with different spatial distance and arrangement. The results of the present study show that the relative distance, number of cylinders in a group and the arrangement both influence the breaking wave force impact on cylinders situated upstream and downstream.

NUMERICAL MODEL

Governing equations

Numerical experiments on focused breaking waves and their interaction with pile groups are investigated in a three-dimensional numerical wave tank using the open-source CFD model REEF3D [22]. The free surface evolution during the entire wave breaking process is calculated. This detail information regarding the impact forces on cylinders and the overturning process of the fo

cused plunging breaking waves is evaluated through turbulence closure achieved through the two equation $k-\omega$ model. Mass and momentum are conserved for the present numerical model by solving the continuity and Reynolds-averaged Navier-Stokes (RANS) equations. The governing equations are denoted as

$$\frac{\partial u_i}{\partial x_i} = 0 \tag{1}$$

$$\frac{\partial u_i}{\partial t} + u_j \frac{\partial u_i}{\partial x_j} = -\frac{1}{\rho}\frac{\partial p}{\partial x_i} + \frac{\partial}{\partial x_j}\left[(\nu + \nu_t)\left(\frac{\partial u_i}{\partial x_j} + \frac{\partial u_j}{\partial x_i}\right)\right] + g_i \tag{2}$$

where u_i is velocity vector (u_1, u_2, u_3) in three-dimension Cartesian coordinate system (x, y, z), t is the time, ρ the fluid density, p the pressure, the pressure gradient is modelled by Chorin's projection method [23] for incompressible flow on a staggered grid. The Poisson equation for pressure is solved using the Bi-Conjugate gradients Stabilised (BiCGStab) struct solver with parallel fully multi-grid (PFMG) pre-conditioner available from the HYPRE solver library. ϕ is the level set function which is a smooth signed distance function $\phi(\vec{x},t)$ to be introduced later. g represents acceleration due to gravity. ν is the kinematic viscosity, and ν_t is the eddy viscosity. The eddy viscosity is determined through the two-equation $k-\omega$ model [24]. The equations for the turbulence kinematic energy k and the specific turbulence dissipation rate ω are as follows:

$$\frac{\partial k}{\partial t} + u_j \frac{\partial k}{\partial x_j} = \frac{\partial}{\partial x_j}\left[\left(\nu + \frac{\nu_t}{\sigma_k}\right)\frac{\partial k}{\partial x_j}\right] + P_k - \beta_k k\omega, \tag{3}$$

$$\frac{\partial \omega}{\partial t} + u_j \frac{\partial \omega}{\partial x_j} = \frac{\partial}{\partial x_j}\left[\left(\nu + \frac{\nu_t}{\sigma_\omega}\right)\frac{\partial \omega}{\partial x_j}\right] + \frac{\omega}{k}\alpha P_k - \beta\omega^2. \tag{4}$$

where P_k represents the turbulent production rate, and the coefficients are defined as $\sigma_k = 2$, $\beta_k = \frac{9}{100}$, $\sigma_\omega = 2$, $\alpha = \frac{5}{9}$, $\beta = \frac{3}{40}$. To avoid the over-production of the eddy viscosity outside the boundary layer, the eddy viscosity is bounded by the eddy-viscosity limiters proposed by [25]:

$$\nu_t = \min\left(\frac{k}{\omega}, \sqrt{\frac{2}{3}}\frac{k}{|\mathbf{S}|}\right) \tag{5}$$

The components of the turbulence near the free surface normal to the surface are damped and redistributed to the ones parallel to the surface, which will be enhanced. To correct the turbulence near the free surface, an additional boundary condition is introduced to give the specific turbulence dissipation term at the free surface and defined as:

$$\omega_s = \frac{c_\mu^{-0.25}}{\kappa} k^{0.5}\left(\frac{1}{y'} + \frac{1}{y^*}\right), \tag{6}$$

with $c_\mu = 0.07$ and $\kappa = 0.4$. The virtual origin of the turbulent length scale y' is empirically found to be 0.07 times the mean water depth [26]. y^* is the distance from the nearest wall.

The specific turbulence dissipation (6) is only activated around the free surface of thickness ε using the Dirac delta function:

$$\delta(\phi) = \begin{cases} \frac{1}{2\varepsilon}\left(1+\cos\left(\frac{\pi\phi}{\varepsilon}\right)\right) & if\ |\phi| < \varepsilon \\ 0 & else \end{cases}, \tag{7}$$

where $\varepsilon = 2.1dx$ and dx is the gird size. ϕ is a level set function which is introduced below.

The governing equations mentioned above are solved for the two-phase flow of air and water. The level set function in a fixed cell $\phi(\vec{x},t)$ is used as a signed distance function which gives the closest distance to the interface and the air and water phases are distinguished by the sign of the values. So the level set function can be expressed with the Eikonal equation $|\nabla\phi| = 1$ and has following properties:

$$\phi(\vec{x},t)\begin{cases} > 0\ if\ \vec{x} \in phase\ 1 \\ = 0\ if\ \vec{x} \in \Gamma \\ < 0\ if\ \vec{x} \in phase\ 2 \end{cases} \tag{8}$$

The free surface Γ evolves over time step and is solved using the velocity field generated by the momentum equation. The convection function for the level set functions is defined as

$$\frac{\partial \phi}{\partial t} + u_j \frac{\partial \phi}{\partial x_j} = 0, \tag{9}$$

The time updating in (9) is solved with the third-order TVD Runge-Kutta scheme [27]. The Hamilton-Jacobi version of the fifth-order Weighted Essentially Non-Oscillatory (WENO) scheme [28] is adopted for the convection terms. The large difference in the density and viscosity at the free surface is handled by smoothening over a region of finite thickness across the interface. This is achieved by defining a smoothed Heaviside function

$$H(\varphi_i) = \begin{cases} 0 & if\ \varphi_i < -\varepsilon \\ \frac{1}{2}\left(1 + \frac{\varphi}{\varepsilon} + \frac{1}{\pi}\sin\left(\frac{\pi\varphi_i}{\varepsilon}\right)\right) & if\ |\varphi_i| \leq \varepsilon \\ 1 & if\ \varphi_i > \varepsilon, \end{cases} \tag{10}$$

Typically the thickness of the smoothed out interface is chosen to be $\varepsilon = 2.1\Delta x$ on both side of the interface. So the material properties of the two phase are determined for the whole simulation domain. The density and viscosity are defined at any location in the domain as

$$\rho_i = \rho_w H(\varphi_i) + \rho_a(1 - H(\varphi_i)), \tag{11}$$

$$\nu_i = \nu_w H(\varphi_i) + \nu_a(1 - H(\varphi_i)), \tag{12}$$

with w indicating water and a air properties. H is the smoothed Heaviside step function in (10). The density is generally determined at the cell faces to get more stable and accurate solution [22].

The governing equations depicted in (1) and (2) are solved with the level set method and $k-\omega$ turbulence model in a finite difference framework. The convection terms of the governing equations are discretised with the fifth-order Weighted Essentially Non-oscillatory (WENO) scheme [29] in the conservative finite-difference framework. A TVD third-order Runge-Kutta explicit time scheme developed by Harten [30] is employed for the time discretisation. The time step is selected following the CFL number with an adaptive time stepping method to satisfy the stability of the simulation while balancing the requirement of the computational cost of the simulation. A Cartesian grid is used in the two-phase flow model for the high-order spatial discretisation schemes. A ghost cell immersed boundary method is employed in REEF3D to incorporate the irregular and non-orthogonal solid boundary conditions.

Numerical Wave Tank

In this paper, wave generation and absorption are carried out using the relaxation method to ascertain good wave quality on generation and absorption of the waves at the end of the domain [31] [32]. Here, the wave generation takes place in a relaxation zone with a typical size of one wavelength. For the numerical beach, the relaxation method is employed in all cases with around two wavelengths. The focused wave generation method is based on the irregular wave theory by adding up of the individual linear harmonic wave components where each of them are of relatively lower amplitude compared to the target focused wave height. The first-order focused wave theory is employed for the free surface defined as

$$\eta^{(1)} = \sum_{i=1}^{N} A_i \cos\theta_i, \tag{13}$$

where, A_i is the amplitude of each wave component and θ_i is the phase of each wave component generated, defined as:

$$\theta_i = k_i x - \omega_i t - \varepsilon_i \tag{14}$$

where ω_i is the angular frequency and k_i is the wave number of each component. The parameter ε_i is the phase angle determined based on the focused specified time t_f and location x_f:

$$\varepsilon_i = k_i x_f - \omega_i t_f \tag{15}$$

Based on the linear superposition theory, the amplitude of each wave component can be expressed in terns of the fixed focused steepness as :

$$A_i = \frac{2\pi S_t}{k_i} \tag{16}$$

where, S_t is the fixed wave steepness of each component and $S_t = \frac{\varepsilon}{2\pi N}$, $\varepsilon = N k_i A_i$ is the initial wave steepness of the target focused wave in the wave generation.

The ghost cell immersed boundary method is used to handle the interface between the solid geometry and the surrounding flow. The wave force on a cylinder is calculated as given below:

$$F_x = \int_\Omega (-\mathbf{n}P + \mathbf{n}\cdot\tau) d\Omega \tag{17}$$

where P is the presure, τ is the viscous stress tensor, $\mathbf{n}$ is the unit normal vector to the surface, pointing out into the ambient fluid domain, and *Omega* is the surface of the solid geometry.

Simulation Setup

The numerical simulation of interaction between the focused plunging breaker and cylinder groups placed in different arrangement are performed in a three-dimensional numerical wave tank using the open-source CFD model REEF3D. The numerical model is validated by comparing the results with the experiment

which carried out by [8] to investigate the impact forces induced by breaking waves on a vertical cylinder in Dalian University of Technology, China. The experiment is conducted in a 20 m long, 0.45 m wide and 0.6 m high glass wall wave tank with water depth $d = 0.3$ m. The vertical cylinder located around in the middle of the wave tank in the experiment. According to the time step convergency of breaking waves calculated by REEF3D, the CFL number is chose as 0.01 as the seen in [16]. Time step is around 0.005s before breaking and 0.004-0.001s during breaking for both cases. For the purpose of optimising the computational cost, the computational domain is 15 m long with $2m$ for wave generation and $3m$ for the wave absorption zone. According to the definition by [33], the moment when the forward wavefront becomes vertical is defined as the incipient breaking point. So the wave gauge is selected at the same position as the experiment breaking position at 9.0 m. The physical set-up of numerical wave tank corresponds to the experiment, which has been shown in the Fig. 1.

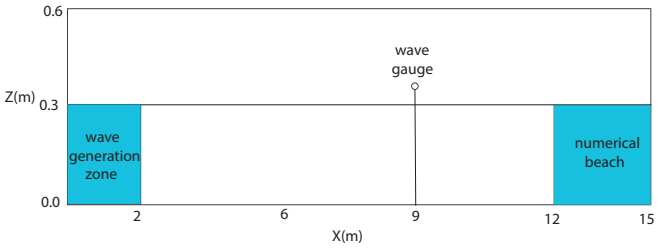

FIGURE 1. Sketch of the numerical wave tank

In order to replicate the experiments, the wave characteristics are kept as the same in the simulations. The focusing wave group has a uniform frequency band ranging from 0.3 Hz to 2.0 Hz. The steepness of the total components $N = 64$ superimposed linearly are $\varepsilon = NA_ik_i$, which is the same and constant for each of the wave components. N is the total number of wave components and k_i is the wave number of ith component given by the linear dispersion relation. The wave height H_w and wave period T at the incipient breaking point are 0.14 m and 1.0 s respectively. The details of the wave group parameters for the focused plunging breaking waves are listed in Table 1.

The scenario where the wave breaks exactly at the cylinder (Fig.2) has been chosen as the wave conditions for all the simulation cases. The incipient breaking point in the simulation is at 9.0 m, therefore, the center of cylinder in the validation case (Fig.3) and the first cylinder in four simulation cases (Fig.4) locate at 9.03 m in X direction and 0.225 m in Y direction. All the vertical cylinders keep the same size as 0.6 m long and diameter $D = 0.06$ m in this study.

TABLE 1. Wave parameters measured at the incident point by wave gauge

F_{range} (Hz)	Wave height H_w(m)	wave period T(Hz)	$\varepsilon = NA_ik_i$	N
0.3-2.0	0.14	1.0	0.48	64

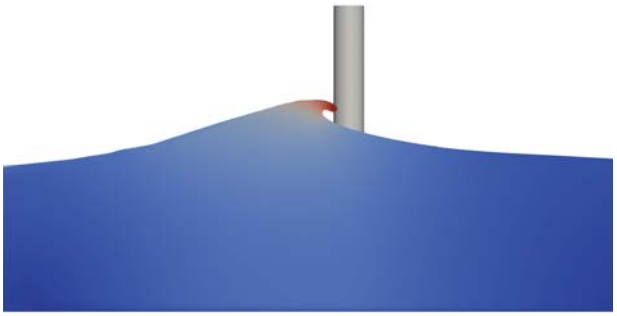

FIGURE 2. Sketch of the scenario for interaction of the breaking waves with cylinder

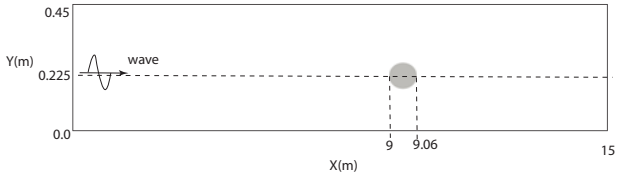

FIGURE 3. The sketch of the validation case set-up

In the present simulations, four cases are arranged to investigate the impact of the plunging breakers on the cylinder groups, as shown in Fig.4. Different pile arrangement including case1- side by side two tandem cylinders with the relative spacing of $S_G = D$, case2- side by side two tandem cylinders with the relative spacing of $S_G = 2D$, case3- three tandem cylinder with the relative spacing of $S_G = D$ and the case4- staggered cylinder group are simulated. The first cylinder in all the cases in Fig.4 is placed in the same position as in the validation case. Within the cylinder group, cylinders are named as cylinder 1, 2, and 3 in sequence from left to right.

RESULTS

Grid convergence and Verification study

The numerical domain is meshed by a stretching grid using the cell size based stretching function. The stretched grids only used

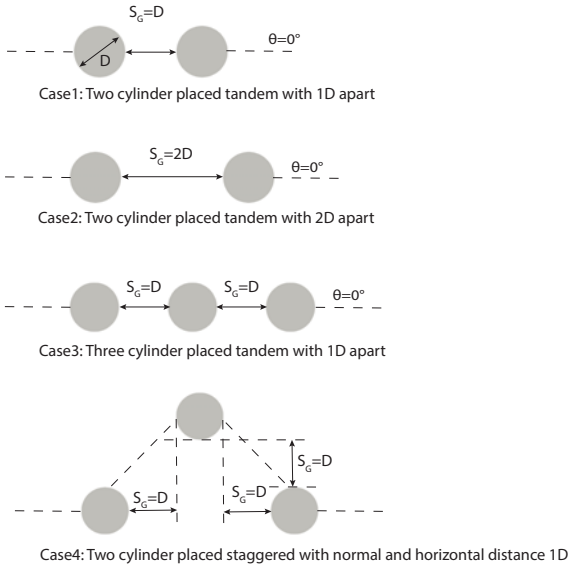

FIGURE 4. The sketch of four cases cylinders arrangement

in the X and Z directions and a uniform grids is used in the Y direction. The grids in X and Z directions are composed of a focused stretching zone and a uniform zone. A uniform cell size of 0.005 m is generated in the focus zone starts from 8.6 m to 9.6 m around the focused wave breaking area in the X direction with 0.01 m uniform grid size outside the focus zone. The focus zone in the vertical direction changes from 0.325 m to 0.475 m with uniform grid size as 0.005 m in the focus zone and 0.01 m outside the focus zone. As the staggered cylinder arrangement and accurate wave force on each of the cylinder group, the grids in the width direction keep the uniform grid size as 0.005 m. There is a short zone between the focused zone and the outside coarse grid zone. The stretched grid of the numerical domain is illustrated in the Fig. 5.

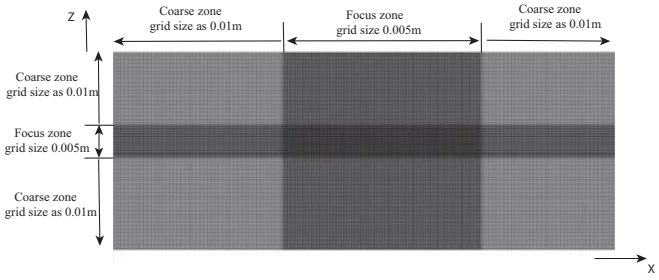

FIGURE 5. Grid stretching arrangement

The grid convergence study and wave elevation validation are carried out using a two-dimensional wave tank. The grid convergence study shows the effect of the grid size arrangement on the results of the interaction of the breaking waves with the vertical cylinder. Fig. 6 shows the comparison of the numerical wave elevation η for the stretching grid and uniform grid size, $dx = 0.02m$, $dx = 0.01m$ and $dx = 0.005m$. The coarse grid size 0.01m and 0.02m fail to capture the wave force accurately. It appears that the waves from the experiments can be reproduced well using this numerical setup with stretching grid changing from 0.005m to 0.01m and uniform grid size $dx = 0.005m$. Therefore, the stretched grids are chosen as the grid arrangement for following simulations.

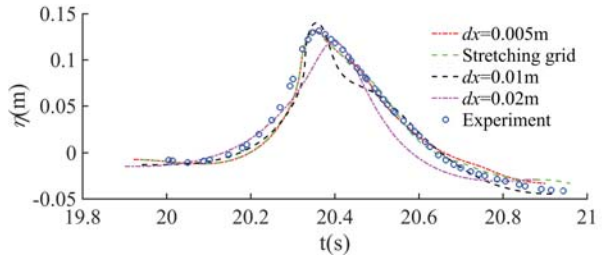

FIGURE 6. Numerical grid refinement study for the focused plunging breaking waves

The free surface elevation at the incipient breaking point provides an expression of the incident wave on cylinder. The comparison of the numerical and experimental wave elevation at the incipient point shows good agreement in Fig.7. The numerical free surface is similar over the wave periods with the experimental data, which indicates that the breaking wave reproduced by the numerical model breaks at the same position with that in experiment.

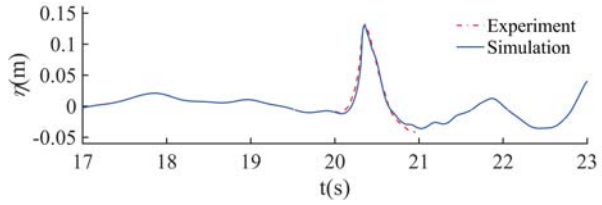

FIGURE 7. Comparison of the numerical results with the experimental wave gauge data at the icipient break point $X_b = 9.0m$

The numerical wave force is compared with the FFT-EMD

treated experimental results resolved by [8] to validate accuracy of the numerical model in the interaction of the breaking waves and the vertical cylinder. Fig.8 shows a good agreement between the numerical and experimental wave forces. The numerical maximum of wave forces on the cylinder occurs at the same time compared to the experimental data, showing that the breaking location predicted by the numerical model is similar to the experimental results. The numerical model can reproduce the wave force induced by the focused plunging breakers on vertical cylinder accurately.

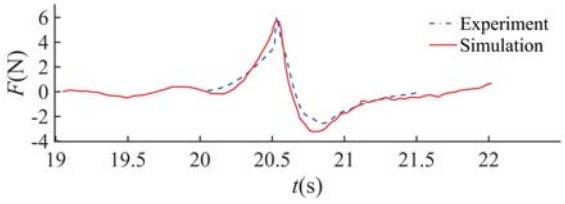

FIGURE 8. Comparison of numerical and experimental wave forces on the vertical cylinder

Focused plunging breaing waves kinematics

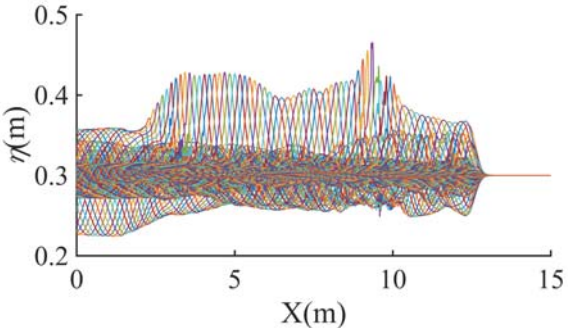

FIGURE 9. Numerical wave elevation along the wave tank for the breaking wave case

The elevation of the wave surface along the wave tank at different time point is shown in Fig.9. In Fig.9 the details of the focused breaking wave generation, evolution, focusing and dispersion are depicted. The wave components interact with each other after the wave generation zone and the wave energy is collected around the focussing position. The height and steepness of the wave elevation increases continuously as the wave components propagating forward interact with each other. The focused wave breaking occurs around 9 m in the wave tank. After the breaking, the free surface elevation decreases instantly.

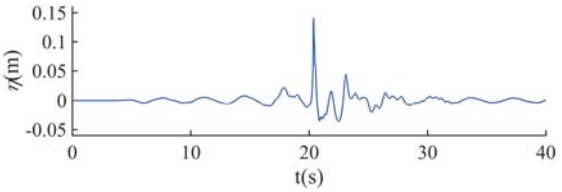

FIGURE 10. Numerical wave surface elevation along time at the icinet breaking point x=9.0m for the breaking wave case

Fig.10 shows the wave elevation measured by the wave gauge located at 9 m the incident point along time series. In Fig.10, the free surface increases instantly around 20 s and then decreases and disperses. The focused wave occurs at 9.0 m around 20 s and only exists for a short time. The process of the focused breaking is shown in Fig.11. At 17 s in Fig.11a, the free surface exceeds the wave breaking limit and the crest of the breaking wave is generated. After that, at 19 s and 21 s in Fig.11b and Fig.11c respectively, the breaking crest continue to evolute. In Fig.11d the crest of the starts to overturn. The maximum velocity magnitude occurs at the crest of the focused breaking wave, which also means that the kinetic energy of the breaking wave is concentrated in the crest. When the crest overturns and rejoins the free surface as shown in Fig.11e, the velocity magnitude on the crest decreases compared to the previous time instant. The air entrainment zone appears and occupies a certain volume in front of the breaking waves after the wave breaking. Fig.11 presents the expression of the plunging breaking phenomenon in detail. The kinematic distribution is also depicted during the breaking process.

Focused breaking waves-cylinder group interaction

The influence of the relative distance and arrangement on the wave forces on cylinders in pile groups are studied in the scenario where the overturning wave crest impacts the first cylinder in the direction of wave propagation at the crest level. Four cases in Fig.4 are conducted in this study. The breaking wave force on a single vertical cylinder is noted as F_0 is regarded as the standard for normalisation, with $F_0 = 6.049N$). The results of the force ratio for these four cases are listed lin Tab.2.

The breaking wave forces on the two tandem cylinders with the relative spacing S_G as $1D$ are presented in Fig.12. For case1, the breaking forces on the cylinder 1 and 2 are $0.92F_0$ and $0.5148F_0$

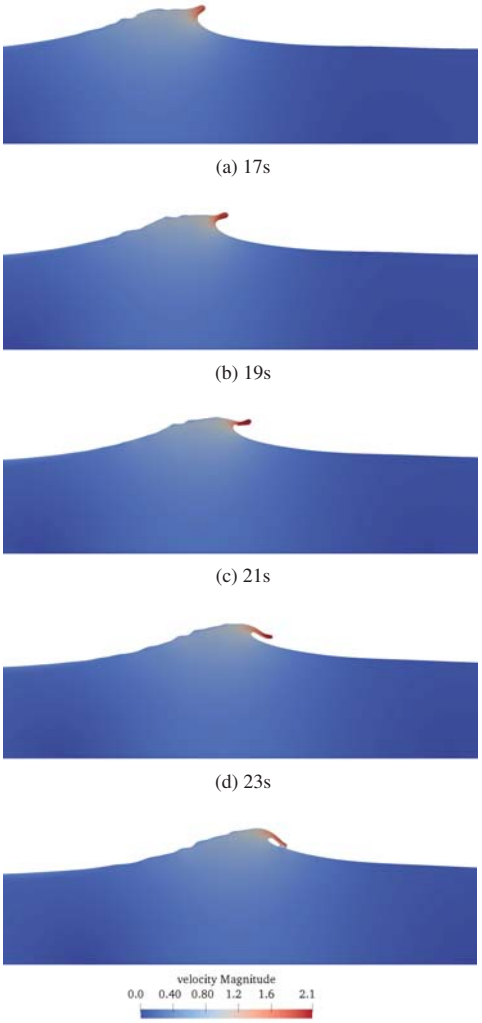

(a) 17s

(b) 19s

(c) 21s

(d) 23s

(e) 25s

FIGURE 11. Free surface profile with velocity magnitude during the breaking process for different time instant

respectively. The wave forces on these two cylinders in case1 have the similar trends. The lowest wave force on each of the cylinders in case1 is the same. The forces on the upstream cylinder are less than that on a single cylinder F_0 due to the effect of reflection from the downstream cylinder. The energy of the breaking waves is dissipated when the waves pass the upstream cylinders. The maximum wave forces on the downstream cylinder are only around half of that on the upstream cylinder as shown in Fig.12.

Fig.13 and Fig.14 capture different perspectives and provide insight into the free surface profile with velocity magnitude during

TABLE 2. Details of the breaking wave force on cylinders

case	S_G	$F_0(N)$	F_1/F_0	F_2/F_0	F_3/F_0
case1	$1D$	6.0493	0.92	0.5148	
case2	$2D$	6.0493	1.05	0.49	
case3	$1D$	6.0493	0.925	0.446	0.56
case4	$1D$	6.0493	1.02	0.816	0.57

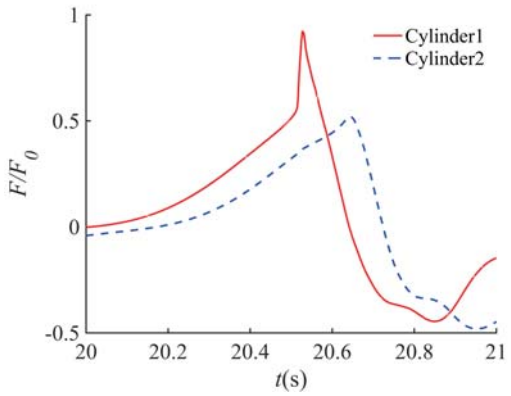

FIGURE 12. Breaking wave forces on two cylinders in case 1

the breaking process for different time instants for case1. The process of the breaking waves from the upstream cylinder to the downstream cylinders are seen in detail. When the breaking wave is close to the upstream cylinder, it attains the maximum values of velocity in Fig.13a and the velocity magnitude decreases in the following time instant. The breaking crest is separated by the first cylinder when it passes the cylinder in Fig.13b. In the top view in Fig.14b, after the breaking waves passes the upstream cylinder, the velocity in the region between the two cylinders is lower compared to the surrounding surface profile. When the broken waves pass the second cylinder, the velocity in the region in between is still lower than the velocity magnitude outside the region between the two cylinders in Fig.13c and Fig.14c. The velocity distribution around cylinders explains the force difference between these two cylinders in case1.

When the relative distance between two tandem cylinders is increased to $2D$ in case2, the wave forces on the upstream cylinder and downstream cylinder are $1.05F_0$ and $0.49F_0$ in Fig.15, respectively. The wave force on the upstream cylinder increase

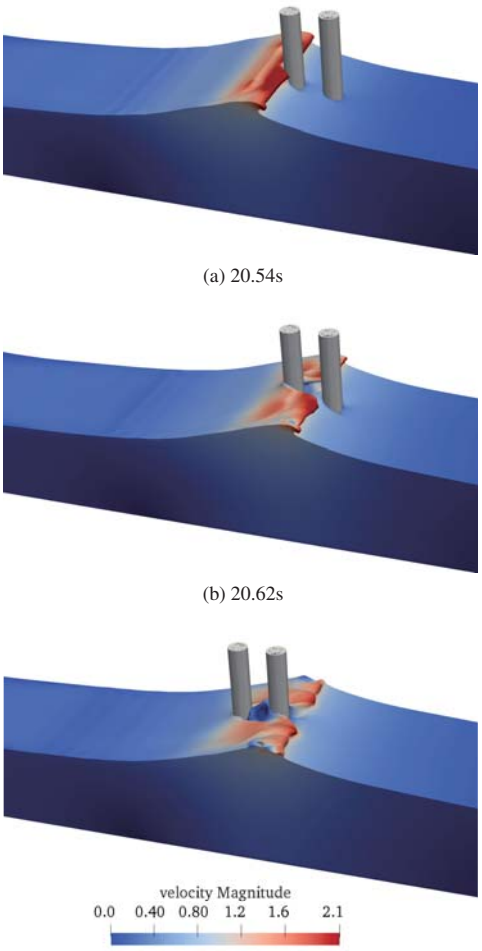

(a) 20.54s

(b) 20.62s

(c) 20.7s

FIGURE 13. Free surface profile with velocity magnitude during the breaking process for different time instant for case 1

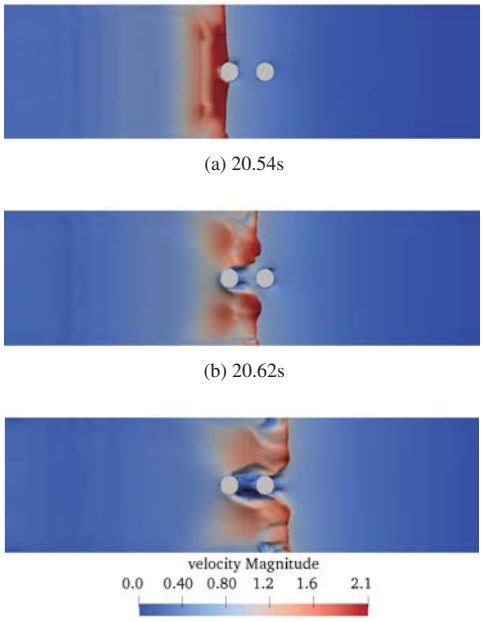

(a) 20.54s

(b) 20.62s

(c) 20.7s

FIGURE 14. Free surface profile with velocity magnitude during the breaking process for different time instant in the top view for case1

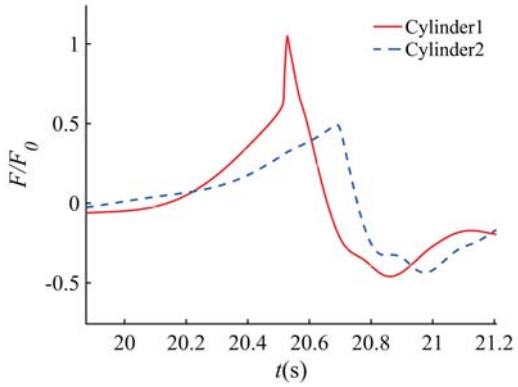

FIGURE 15. Breaking wave forces on two cylinders in case 2

but the shape of the force line does not change. The wave forces on the downstream cylinder show a decrease compared to the downstream cylinder in case1. The maximum wave forces are affected by the relative distance of the cylinders in pile group.

The simulated wave force on three tandem cylinders with relative spacing $S_G = 1D$ are shown in Fig.16. The wave forces on the side by side cylinder 1, cylinder 2 and cylinder 3 are $0.925F_0$, $0.446F_0$ and $0.56F_0$ respectively. Compared to the second cylinder in case1, the wave forces on the cylinder in the middle in case 3 are decreasing due to the influence of the third cylinder. The presence of cylinder 3 influences the wave forces on the cylinder 2 in case 3 and vice versa. However, this arrangement of the cylinder group does not show a lot of influence on the wave forces on the first cylinder. The wave force on the second cylinder is the lowest in case3, which may indicate that a partial influence of the neighbouring cylinders.

Breaking wave interaction with side by side three tandem cylinders contoured by the velocity magnitude are shown in Fig.18 and Fig.19. The incident wave impacts the first cylinder with the highest velocity values at the wave crest in Fig.18a. The incident wave is broken and interacts with the second cylinder in Fig.18b. The wave crest besides the zone in between the cylin-

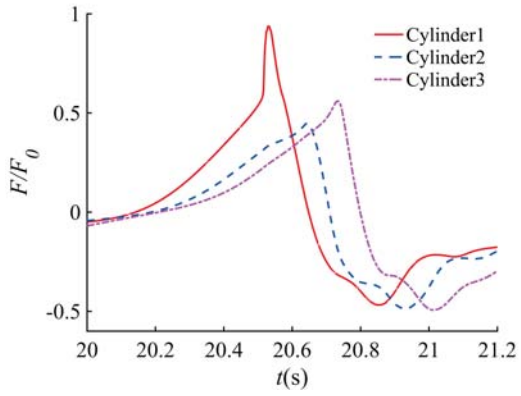

FIGURE 16. Breaking wave forces on two cylinders in case 3

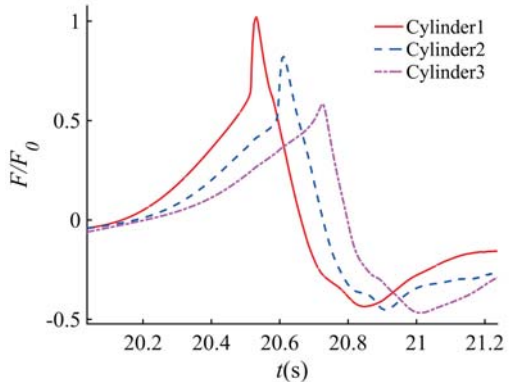

FIGURE 17. Breaking wave forces on two cylinders in case 4

ders continues to overturn in Fig.18b. The region of separation between cylinder 1 and 2 becomes larger in Fig.18c compared to that in Fig.18b. After the broken wave passes cylinder 2, two broken waves move around cylinder 2 and meet as they interact with cylinder 3 in Fig.18d. The reunion of the broken crest results in larger wave forces on cylinder 3 compared to cylinder 2. From the top view in Fig.19, it is apparent that the velocity magnitude on the crest is decreasing continually. The flow structures change instantly when the breaking wave passes the cylinders. The maximum velocity distributed with the shape as 'Ω' around cylinders.

The wave forces on the staggered three cylinders in case 4 are shown in Fig.17. The values of the wave forces on these three cylinders are $1.02F_0$, $0.816F_0$ and $0.57F_0$ in the sequence for cylinder 1, 2 and 3. The changes to the arrangement from tandem to staggered effects the force distribution on cylinders in the group. The location of the middle cylinder significantly in-

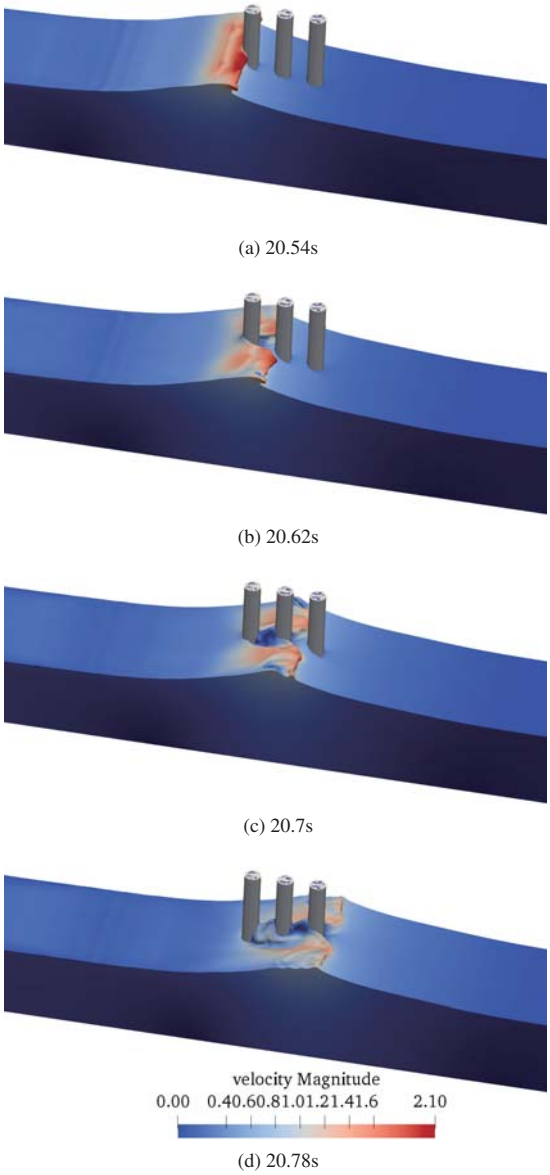

FIGURE 18. Free surface profile with velocity magnitude during the breaking process for different time instant for case 3

fluences the wave forces on cylinders 1 and 2. Compared with cylinders in case 3, the forces on the cylinder 1 and cylinder 2 are both increase. The values of cylinder 2 in case4 are almost twice compared to cylinder 2 in case 3. The details of the interaction are shown in Fig.20. The interaction of the incident wave and cylinder 1 in Fig.20a is the same as that in case3. After the breaking wave passes cylinder 1, the broken wave and the water jet interact with cylinder 2 located in the direction of 45°. The

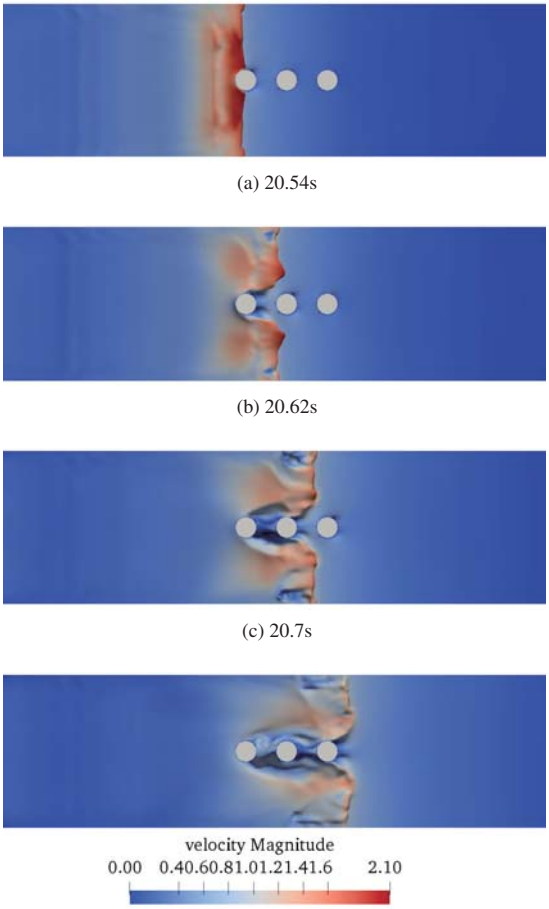

(a) 20.54s

(b) 20.62s

(c) 20.7s

(d) 20.78s

FIGURE 19. Free surface profile with velocity magnitude during the breaking process for different time instant in the top view for case 3

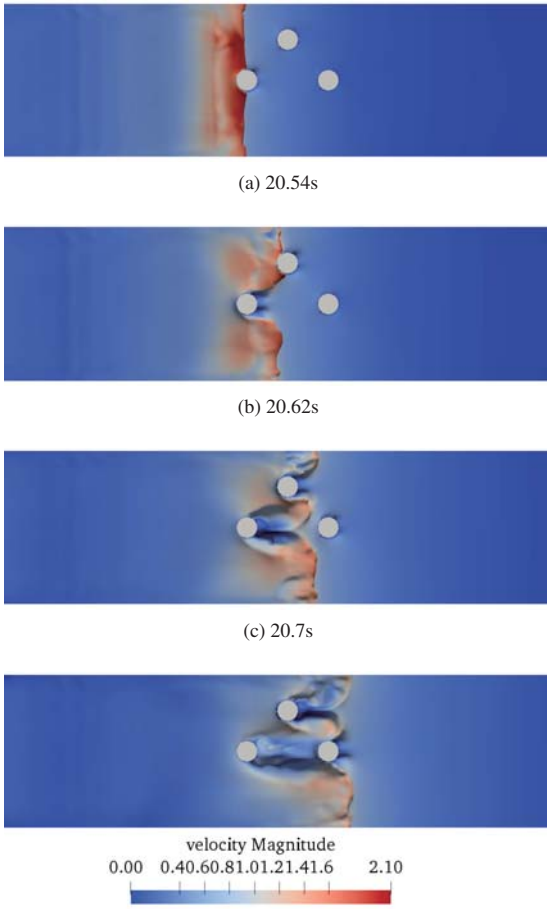

(a) 20.54s

(b) 20.62s

(c) 20.7s

(d) 20.78s

FIGURE 20. Free surface profile with velocity magnitude during the breaking process for different time instant for case 4

broken waves passing cylinder 1 and 2 meet in front of cylinder 3 in Fig.20c. The flow structure is more complex in the staggered arrangement compared to that in the tandem arrangement.

CONCLUSIONS

Numerical simulations of the interaction between the focused plunging breaking waves and four cylinders in pile groups have been conducted using the open-source CFD model REEF3D. The two-phase flow is modelled using the RANS equations and two-equation $k-\omega$ turbulence models. The numerical model is validated by comparing the numerical free surface elevation and wave forces with the experimental data for the plunging breaker impact on a single vertical cylinder at DUT. The comparison shows that the results obtained by numerical simulation shows good consistency with experiments. The purpose of this study is to study the interactions between plunging breakers and the pile group The influence of relative distance between cylinders, number of cylinders and the arrangement on the breaking wave forces on the cylinders inside the pile group are also considered in this study. The four cases are carried out to calculate the breaking wave force on each of cylinders in the group and analyse the interaction between cylinders. The kinematics of the flow field during the process of the breaking waves passing the cylinder group are contoured by the velocity magnitude and discussed with the relationship among the wave force on cylinders. The following conclusions are drawn from the results:

1. The relative distance between two cylinders effects the wave forces on the neighbouring cylinders. Besides, the distance also influences the velocity and flow field in the region between two cylinders. The wave forces on the second cylinder in tander

arrangement when the incident wave crest impacts on the first cylinder are almost half of that on the upstream cylinder.
2. The breaking waves pass the first cylinder and result in broken waves and water jets. The profile of these phenomena plays a major role in the wave forces on the second cylinder. The wave force on the cylinder located at these water jets is higher than that on the cylinder directly behind the first cylinder. The reunion and interaction of these features effects the wave force on the neighbouring cylinders.
3. The third cylinder shows lesser influence on the first cylinder. The interaction of cylinders occurs mostly when they are direct neighbours. The arrangement of the cylinder group influences the force distribution on each of the cylinders. The velocity distribution of the flow field provides an insight into the interaction of the breaking waves and the cylinder group.

ACKNOWLEDGEMENTS

The computations were performed on resources provided by UNINETT Sigma2 - the National Infrastructure for High Performance Computing and Data Storage in Norway under project no. NN2620K.

REFERENCES

[1] Morison, J., O'brien, M., Johnson, J., and Schaaf, S., 1950. "The force exerted by surface waves on piles". *Am Inst Min Metall Eng,* ***189***, 01, pp. 147–154.
[2] Goda, Y., Haranaka, S., and Kitahata, M., 1966. "Study on impulsive breaking wave forces on piles". *Report Port and Harbour Technical Research Institute,* ***6***, 01, pp. 1–30.
[3] Sawaragi, T., and Nochino, M., 1984. "Impact forces of nearly breaking waves on a vertical circular cylinder". *Coastal Engineering Journal,* ***27***, 12, pp. 249–263.
[4] Swift, R., 1989. "Prediction of breaking wave forces on vertical cylinders". *Coastal Engineering,* ***13***(2), pp. 97 – 116.
[5] Watanabe, A., and Horikawa, K., 1974. "Breaking wave forces on a large diameter cell". pp. 1741–1760.
[6] Wienke, J., and Oumeraci, H., 2005. "Breaking wave impact force on a vertical and inclined slender pile—theoretical and large-scale model investigations". *Coastal Engineering,* ***52***(5), pp. 435 – 462.
[7] Zang, J., Taylor, P., and Tello Ruiz, M., 2010. "Steep wave and breaking wave impact on offshore wind turbine foundations - ringing revisited".
[8] Tai, B., Ma, Y., Niu, X., Dong, G., and Perlin, M., 2019. "Experimental investigation of impact forces induced by plunging breakers on a vertical cylinder". *Ocean Engineering,* ***189***, 10, p. 106362.
[9] Ning, D., Zang, J., Liu, S., Taylor, R., Teng, B., and Taylor, P., 2009. "Free surface evolution and wave kinematics for nonlinear uni-directional focused wave groups". *Ocean Engineering,* ***36***, 11, pp. 1226–1243.
[10] Fernández, H., Sriram, V., Schimmels, S., and Oumeraci, H., 2014. "Extreme wave generation using self correcting method - revisited". *Coastal Engineering,* ***93***, 11, p. 15–3.
[11] Bonakdar, L., and Oumeraci, H., 2015. "Pile group effects on the wave loading of a slender pile: A summary of laboratory investigations".
[12] Xie, Z., Lu, L., Stoesser, T., Lin, J.-g., Pavlidis, D., Salinas, P., Pain, C., and Matar, O., 2017. "Numerical simulation of three-dimensional breaking waves and its interaction with a vertical circular cylinder". *Journal of Hydrodynamics,* ***29***, 10, pp. 800–804.
[13] Lin, P., and Liu , P., 1998. "A numerical study of breaking waves in surf zone". *Journal of Fluid Mechanics,* ***359***, 03, pp. 239 – 264.
[14] Bihs, H., Kamath, A., Alagan Chella, M., and Arntsen, Ø. A., 2018. "Extreme wave generation, breaking, and impact simulations using wave packets in reef3d". *Journal of Offshore Mechanics and Arctic Engineering,* ***141***, 12.
[15] Bihs, H., Alagan Chella, M., Kamath, A., and Arntsen, Ø. A., 2017. "Numerical investigation of focused waves and their interaction with a vertical cylinder using REEF3D". *Journal of Offshore Mechanics and Arctic Engineering,* ***139***, 03.
[16] Kamath, A., Alagan Chella, M., Bihs, H., and Arntsen, Ø. A., 2016. "Breaking wave interaction with a vertical cylinder and the effect of breaker location". *Ocean Engineering,* ***128***, 12.
[17] Kamath, A., Alagan Chella, M., Bihs, H., and Arntsen, Ø. A., 2015. "Evaluating wave forces on groups of three and nine cylinders using a 3d numerical wave tank". *Engineering Applications of Computational Fluid Mechanics,* ***9***, 07, pp. 1–12.
[18] Kamath, A., Alagan Chella, M., Bihs, H., and Arntsen, Ø. A., 2015. "CFD investigations of wave interaction with a pair of large tandem cylinders". *Ocean Engineering,* ***108***, 11, pp. 738–748.
[19] Bihs, H., 2017. *DIVEMesh :: User's Guide*. Department of Civil and Environmental Engineering, NTNU Trondheim.
[20] Bihs, H., Kamath, A., Alagan Chella, M., and Arntsen, Ø. A., 2016. "Breaking-wave interaction with tandem cylinders under different impact scenarios". *Journal of Waterway Port Coastal and Ocean Engineering,* ***142***, 03, p. 04016005.
[21] Alagan Chella, M., Bihs, H., Kamath, A., Myrhaug, D., and Arntsen, Ø. A., 2019. "Breaking wave interaction with a group of four vertical slender cylinders in two square arrangements". *Journal of Offshore Mechanics and Arctic Engineering,* ***141***, 04.
[22] Bihs, H., Kamath, A., Alagan Chella, M., Aggarwal, A., and Øivind A. Arntsen, 2016. "A new level set numerical

wave tank with improved density interpolation for complex wave hydrodynamics". *Computers Fluids,* ***140***, pp. 191 – 208.

[23] Chorin, A. J., 1968. "Numerical solution of the navier-stokes equations". *Mathematics of Computation,* ***22***(104), pp. 745–762.

[24] Wilcox, D. C., 1988. "Reassessment of the scale-determining equation for advanced turbulence models". *AIAA Journal,* ***26***(11), pp. 1299–1310.

[25] Durbin, P., 2009. "Limiters and wall treatments in applied turbulence modeling". *Fluid Dyn Res,* ***Volume 41***, pp. 1–18.

[26] Hossain, M., and Rodi, W., 1980. Mathematical modeling of vertical mixing in stratified channel flow. Second Symposium on Stratified Flows, Trondheim, Norway.

[27] Gottlieb, S., and Shu, C.-W., 1998. "Total variation diminishing runge-kutta schemes". *Math. Comput.,* ***67***(221), Jan., p. 73–85.

[28] Jiang, G.-S., and Peng, D., 2000. "Weighted eno schemes for hamilton–jacobi equations". *SIAM Journal on Scientific Computing,* ***21***(6), pp. 2126–2143.

[29] Jiang, G.-S., and Shu, C.-W., 1996. "Efficient implementation of weighted eno schemes". *Journal of Computational Physics,* ***126***(1), pp. 202 – 228.

[30] Shu, C.-W., and Osher, S., 1988. "Efficient implementation of essentially non-oscillatory shock-capturing schemes". *Journal of Computational Physics,* ***77***(2), pp. 439 – 471.

[31] Mayer, S., Garapon, A., and Sørensen, L., 1998. "A fractional step method for unsteady free-surface flow with applications to non-linear wave dynamics". *International Journal for Numerical Methods in Fluids,* ***28***(2), pp. 293–315. cited By 150.

[32] Jacobsen, N. G., Fuhrman, D. R., and Fredsøe, J., 2012. "A wave generation toolbox for the open-source cfd library: Openfoam®". *International Journal for Numerical Methods in Fluids,* ***70***(9), pp. 1073–1088.

[33] Bonmarin , P., 1989. "Geometric properties of deep-water breaking waves". *Journal of Fluid Mechanics,* ***209***, pp. 405 – 433.